BIM-GIS Modelling for Sustainable Urban Development

clean technologies

MDPI

Article

Design of a Solar Dish Receiver and Life Cycle Assessment of a Hot Water System

Ibrahim Tursunović [1] and Davide Papurello [1,2,*]

[1] Department of Energy (DENERG), Politecnico di Torino, Corso Duca Degli Abruzzi, 24, 10129 Turin, Italy
[2] Energy Center, Politecnico di Torino, Via Paolo Borsellino 38/16, 10138 Turin, Italy
* Correspondence: davide.papurello@polito.it

Abstract: The energy sector is the main source of greenhouse gases, so it has the highest potential for improvement. The improvements can be achieved by generating energy from renewable sources. It is necessary to combine production from renewable sources with storage systems. Thermal energy storage using concentrated solar power systems is a promising technology for dispatchable renewable energy that can guarantee a stable energy supply even in remote areas without contributing to greenhouse gas emissions during operation. However, it must be emphasised that greenhouse gases and other impacts can occur during the production process of concentrating solar system components. This paper analyses the receiver design to produce thermal energy for the existing CSP dish plant at the Energy Center of the Politecnico di Torino. The plant is designed to produce electrical energy in the spring and summer periods. In addition to this energy production, the CSP can be adopted to produce thermal energy, through hot water, during the less favourable periods of the year in terms of global solar radiation. The surface heat flux is calculated in the first part of the analysis to obtain the maximum internal temperature in the receiver, which is 873.7 °C. This value is a constraint for the choice of material for the solar receiver. A life cycle assessment is performed to compare the emissions generated during the production of the main components of the CSP system with the emissions generated by the methane-fuelled water heater to produce the same amount of thermal energy. It can be concluded that the production of the main components of the CSP system results in lower greenhouse gas emissions than the operational phase of a conventional system. Given the assumptions made, the utilization of methane leads to the emission of approximately 12,240 kg of CO_2, whereas the production of the CSP system results in emissions totalling 5332.8 kg of CO_2 equivalent.

Keywords: LCA; CSP; solar energy; domestic hot water; renewable energy

Citation: Tursunović, I.; Papurello, D. Design of a Solar Dish Receiver and Life Cycle Assessment of a Hot Water System. *Clean Technol.* **2024**, *6*, 379–396. https://doi.org/10.3390/cleantechnol6010019

Academic Editor: Constantinos V. Chrysikopoulos

Received: 18 December 2023
Revised: 29 February 2024
Accepted: 15 March 2024
Published: 19 March 2024

1. Introduction

The European Green Deal aims to make Europe the first carbon-neutral continent by 2050 and to reduce greenhouse gas emissions by at least 55% by 2030 [1]. These goals are achievable through a broad energy transition in different sectors. Five emission sectors have been identified, and in Europe, the main one is transport (28%) [2]. The widely studied and debated energy transition will bring many benefits, such as increased energy reliability, economic growth, and job creation [3,4]. Gielen et al. pointed out that the use of renewable energies, and improved conversion factor, together with the electrification of end uses, account for 94% of emission reductions [3]. Although energy use for heating has remained stable since 2010, production systems are mostly powered by fossil fuels. The share powered by renewable energy was around 20% in 2019 [5]. To reach the goals of the Sustainable Development Scenario (SDS), clean energy technologies must exceed 50% of new heating equipment sales by 2030 [6]. Heating and hot water account for 79% of total final energy use in EU countries [7]. Solar energy, in particular concentrated solar power (CSP), can play a crucial role in this context, especially for district heating networks [8–11]. Solar energy is

used in solar district heating (SDH) projects across Europe, contributing up to 20% of annual heat demand, and potentially more with seasonal storage [12]. Among CSP technologies, the dish system offers high thermal efficiency for medium-to-high temperatures and is suitable for high-temperature applications [13]. Efficient energy conversion is achieved with sun-tracking parabolic dish collectors and cavity receivers, minimizing heat losses [14]. Parabolic collectors show superior energy conversion efficiency among CSP systems, as studied by Coventry et al. [15]. However, each dish has a relatively low heat output, often in the order of tens of kilowatts. A positive aspect is the possibility of producing thermal and electrical energy in a combined manner. These features make dishes particularly interesting for domestic applications, small buildings, and local communities. However, dish technology is not widely adopted, and the stability of conversion efficiency needs to be extended to increase commercial penetration [16]. Only a few studies focus on the heating part of CSPs [15,17,18]. Coventry et al. highlighted the operation of thermal energy of a CSP system (2016), where an output of the system in addition to electricity is also the production of pressurised hot water, which can be used in a thermal energy distribution network [15]. This study is mainly concerned with evaluating the performance of an existing CSP dish located at the Energy Center of Turin. One of the main objectives of this study is to evaluate the production of thermal energy in the winter and autumn seasons. The solar concentrator has its normal operation in producing electricity from the accumulation of concentrated solar radiation in the receiver. This occurs most easily in the seasons from spring to autumn. The production of thermal energy is a surplus that is added to the production of electricity [19–22]. In this study, the CSP dish is integrated with a water storage tank, forming a system designed to provide hot water for integration into the Energy Centre's network. In the second part of the paper, a comprehensive life cycle analysis (LCA) will be conducted on the key components of the entire system used. In particular, the proposed configuration does not incorporate any fossil-based backup heating sources, ensuring no pollutant emissions during the system operation. Thus, the innovative part of the study concerns not only the production of renewable energy from concentrated solar power, but also the life cycle analysis for each plant component. In this analysis, the solar collector, the solar receiver, the domestic hot water tank, and the piping system are included.

2. Material and Methods

The concentrator consists of a single solar dish with an aperture of approximately 2.4 m (Elma net. Srl, Trento, Italy). The system is composed of two motors to allow optimal orientation according to the time of day, and from the geographical coordinates of the site where the CSP is installed (Turin, 45.0676° N, 7.6563° E). Other useful geometric and technical parameters are listed in the following table (Table 1) and in previous studies [21,23].

Table 1. Features of the solar dish concentrator.

	Description	Value	Unit of Measure
D_c	Diameter of the dish	2370	mm
f	Focal distance	958	mm
y_R	Depth	370	mm
$\boldsymbol{\varphi_R}$	Rim angle	61.89	°
Co	Optical concentration ratio	8013	-
d_f	Diameter of the focal point	6.41	mm
l	Length of the receiver	200	mm
A	Area of the concentrator	4.5	m^2
P	Power of the concentrator	2.8	kW

The concentrator–receiver system is built using the Comsol Multiphysics 5.6 Inc. software (Burlington, MA, USA). In this study, the global irradiance varied from 350 to 800 W/m^2, in the autumn and winter seasons. This value is derived from previous experimental measurements conducted in the plant and recently published [19]. If the dish were a perfect reflector, i.e., if all incoming radiation were reflected specularly, if the dish were perfectly smooth, and if the sun's rays behaved as planar waveforms from an infinitely distant point source, all incoming rays would focus on a single point in the collector—in the focus of the paraboloid. To make the system more realistic, some deviations from the ideal case were included in the analysed model:

- Part of the incident radiation is absorbed by the dish. In this model, the absorption coefficient is set to 0.1, which means that 90% of the incoming radiation is reflected [24].
- Not all incident rays will be parallel; on the contrary, incident rays are sampled by a narrow cone with a maximum angle, ψm, of 4.56 mrad [24]. A part of the radiation is also emitted from the circumsolar region surrounding the solar disc, instead of from the solar disc itself, but this radiation is neglected in the present model, i.e., a circumsolar ratio (CSR) of zero is assumed.
- The reflected rays are not all released in the same direction because the surface of the parabola is not smooth. Instead, the normal to the surface is perturbed by an additional angle that is sampled by a Rayleigh distribution. This optical error is considered with a surface tilt error of 1.75 mrad [24].
- The limb-darkening effect is considered to consider the variation in power of rays from different regions of the Sun. Rays emitted from the centre are more intense than those emitted from the peripheral regions of the solar disc.
- Rays are released from 250,000 distinct points (limitations due to computational costs influenced by the nature of the computer).

The limb-darkening effect is used to consider the non-uniform distribution of solar radiation across the solar disc, considering that the intensity of sunlight varies from the centre to the outer regions of the solar disc. This variation can be influenced by factors such as the angle of incidence and the solar temperature profile.

In the present study, a cavity solar receiver was chosen for its simplicity and ease of fabrication, see Figures 1 and 2. The mesh must have a higher resolution on curved surfaces to accurately represent the surface normal. On the other hand, the mesh on flat surfaces can be coarser. A fine mesh on curved surfaces improves the accuracy of the reinitialised wave vectors of reflected and refracted rays [25]. To reduce the mesh size on the curved surfaces without creating superfluous meshes, 0.2 as the curvature factor was selected. Furthermore, since the main objective is to determine the temperature distribution within the receiver, a customised free triangular mesh was used on the receiver with a maximum element size of 0.0002 [mm] and a minimum element size of 0.00004 [mm].

The shape and dimensions of the receiver, the solar absorptance of its inner surface, and the type of reflection on its inner surface, in conjunction with the parameters introduced earlier, collectively influence the uneven absorption of heat flux by the receiver's inner surface. These factors play a crucial role in determining the actual distribution of absorbed radiant flux density.

The mesh independence analysis was accomplished using the same procedure reported in Marra et al. [19]. The model built was validated with experimental temperature measured inside the receiver structure using a B-type thermocouple (Tersid srl, Milan, Italy) [26]. The system modelled (CSP + cavity receiver) is connected to a water storage tank to meet the hot water needs for a single family of four persons, for more details refer to [27]. Thermal demand for domestic hot water is expressed by the following equation:

$$Q_{DHW} = \dot{m} \cdot c_p \cdot (T_{use} - T_{mains}) \quad (1)$$

where $\dot{m}$ is daily demand of DHW in $\frac{kg}{s\ person}$; and temperature, T_{use}, can be generally assumed to be in the range of 40 $\div$ 50 °C. However, temperature from the aqueduct is

related to the average temperature of the ground at $1 \div 2\ m$ depth. In Italy, T_{mains} varies between 12 and 14 °C in the Po valley. The demand for the DHW is equal to around 27,000 $\frac{kJ}{day}$ or 7.5 $\frac{kWh}{day}$ for the selected case study. An important aspect related to the performance of a TES is maintaining a high degree of stratification of the reactor volume connected to the users. Thermal stratification allows a limited operation of auxiliary energy supply. For sensible TES, the lower and upper-temperature limits determine the maximum capacity stored. Thus, maximum storage capacities are not accessible in real storage systems [28].

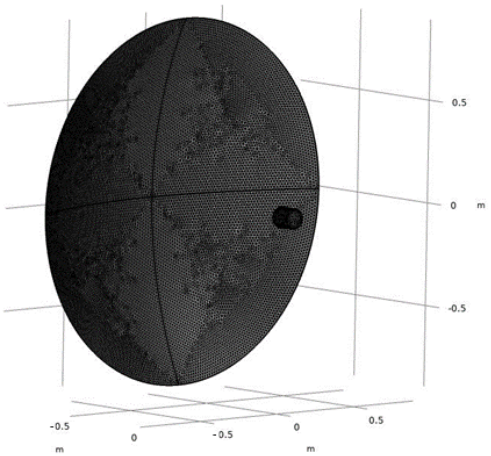

Figure 1. Mesh representation of the CSP with the cavity receiver in the Comsol multiphysics software.

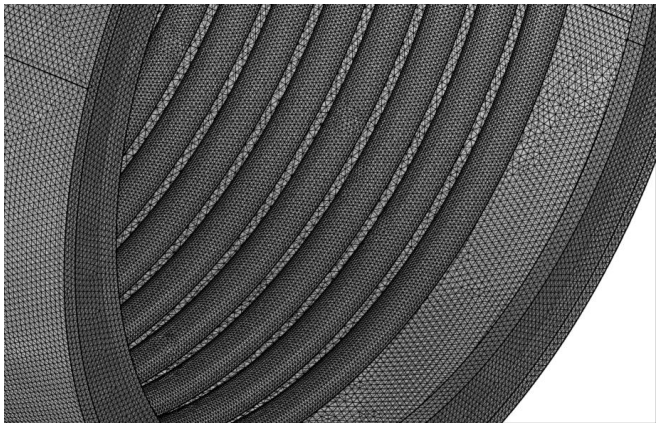

Figure 2. Mesh representation of the receiver's inner surface.

The size of the storage is based on the following equation:

$$V = \frac{Q}{\rho \cdot c_p \cdot (T_{max} - T_{min})} \tag{2}$$

where Q is the thermal energy demand, T_{max} is the maximum temperature in the tank ($80 \div 85$ °C for non-pressurized water tank), and T_{min} is the minimum temperature for satisfying the demand ($45 \div 55$ °C) [28]. In this study, the maximum tank temperature was set at 80 °C (to prevent legionella) and the minimum at 45 °C, and, using the previously calculated hot water demand, a volume of 190 L was sufficient. The energy demand for heating this volume of water can be evaluated by the following equation:

$$E = m \cdot c_p \cdot \Delta T \tag{3}$$

where E is the amount of thermal energy required to heat water, m is the water tank volume, c_p is the specific heat of the water, and ΔT is equal to 15 °C.

$$E = 190 \times 1.16 \times 10^{-3} \times 35 = 7.71 \text{ kWh} \quad (4)$$

In the second part of the paper, a life cycle analysis was performed. Despite the widespread use of concentrated solar power plants, their environmental assessment is still little investigated. Reviewing the literature studies on the LCA of CSP, it can be seen that most of the references concern CSP plants based on parabolic troughs and solar tower technology [29–31]. Leamnatou et al. state that the impact of CSP plants depends on the use of water and the materials used for storage. Carnevale et al. presented a general case of LCA of solar energy systems [32,33]. By reviewing the literature, further investigations are needed on plate systems, storage materials, water-saving strategies, and the soiling effect, for even small systems focused on small CSP systems.

This analysis aims to study the impacts of a solar dish (CSP) used for cradle-to-grave energy production, as no similar studies exist in the literature. The LCA analysis is performed on the macro-components of the system. These components are the solar dish, the solar receiver, the water storage tank, and the piping. This choice is due to several limitations, one of which is the database used. Since the database has limited sources, the electronic components were excluded from the analysis—the same applies to the soldering of the parts. The functional unit chosen in this study is "a hot water tank", and, following ISO standards 14040 and 14044, the results of the LCA are expressed in terms of this functional unit.

The system boundary shown in Figure 3 includes the production, utilisation, and final decommissioning phases. Four different processes were considered separately to produce the system.

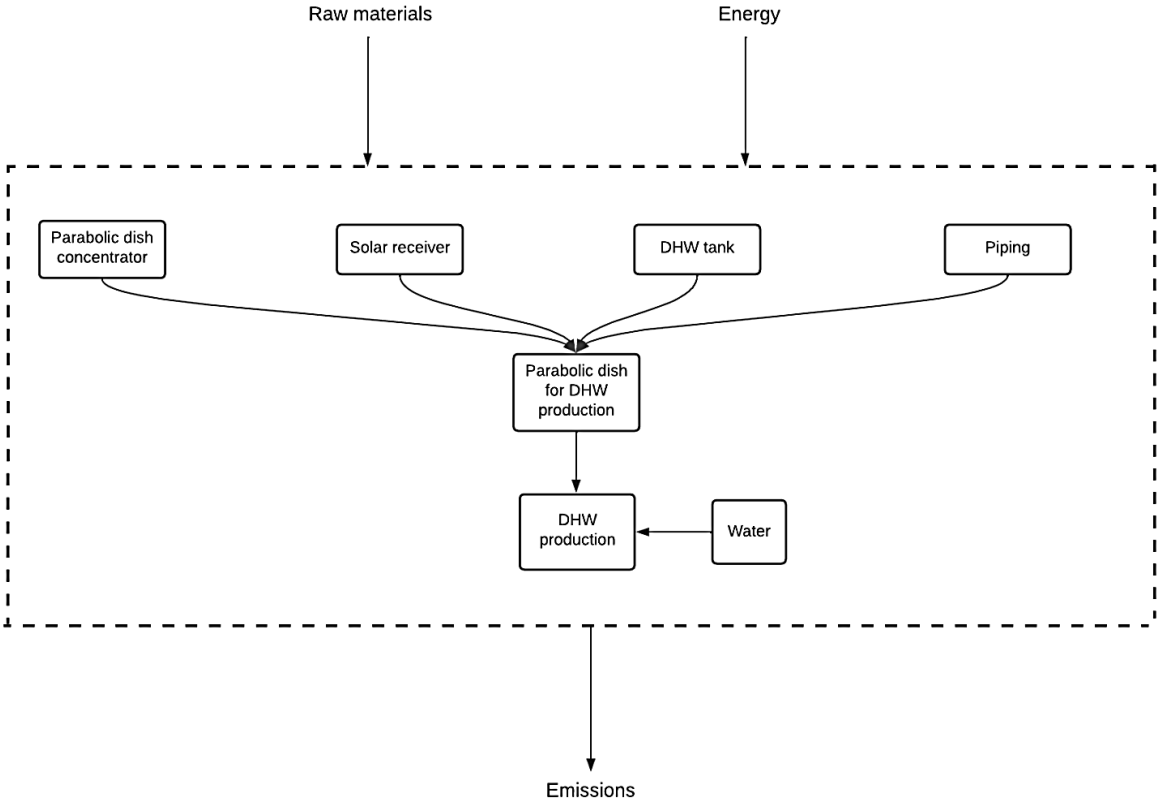

Figure 3. LCA boundary system representation.

Each process includes raw material extraction and end-of-life treatment. The process "parabola for hot water production" represents a process that includes all the outputs of the previous processes. It includes four upstream processes as inputs and their transport from the production site to the utilisation site. The output of the process "parabola for domestic hot water production" is the input of "domestic hot water production", together with "water". The last process is the functional unit to which all results will be referred: a domestic hot water tank. In this last process, which represents the utilisation phase, water consumption is also included. In this case, the transport of water from the extraction source to the point of use is not considered. The manufacturing processes of the hot water tank, receiver, piping, and solar collector do not include the impacts of their assembly. These impacts were omitted due to a lack of reliable data. Furthermore, due to the difficulty of finding accurate information on the quantities of materials used, the analysis was based on product data sheets and estimates from the literature. The life expectancy of the components is assumed to be 30 years (30 years $\times$ 365 days per year = 10,950 days). If the tank operates for 255 days per year (due to non-continuous use for 12 months) and considering, the previously introduced functional unit "a domestic hot water tank", the weight of one day of operation is equal to 0.000131 of the life expectancy (1/7650 days (7650 days = 30 years $\times$ 255 days/year)), see Figure 4. Certainly, within the lifetime estimated by the manufacturer of the solar concentrator (Elma net. Srl, Trento, Italy) are already included several installations for the replacement of major components subject to wear and tear, including the coating of the solar disc and the overhaul of the two motors required for solar tracking. Here, the flow chart of the system is presented starting from the raw material extraction, considering the energy production reaching the end of life of the system. Since the solar disk is in Turin, Italy, whenever possible, the processes used for data representation were in Italy, Europe, or a European country. The software used is openLCA 1.10.3 (GreenDelta GmbH, Kaiserdamm, Berlin, Germany), and the database is version 1.00 of the open-source Environmental Footprint database.

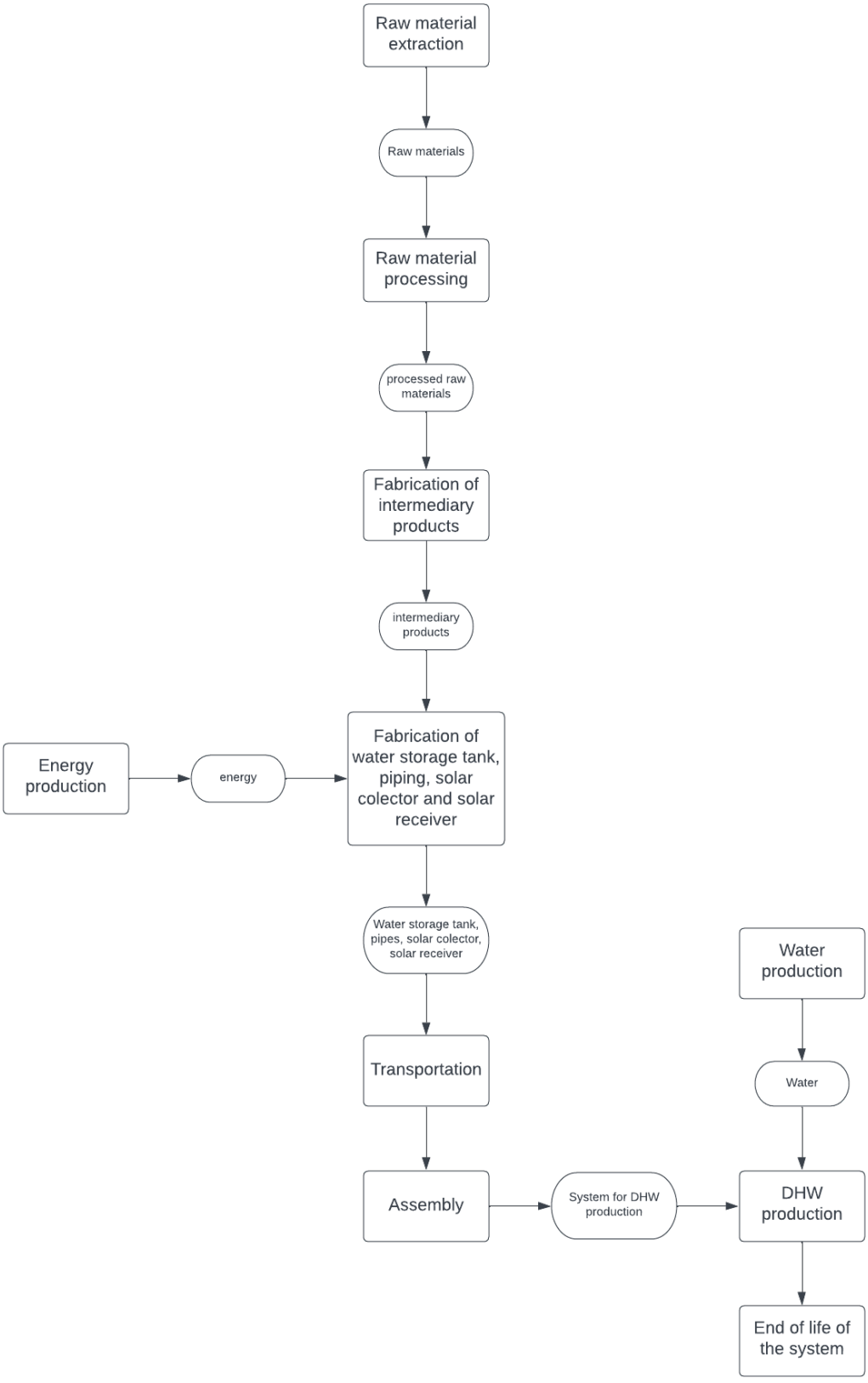

Figure 4. Flowchart of the system.

3. Results and Discussion

3.1. Material Selection and Quantification for LCA

The tanks used to contain the water are made of steel with cathodic corrosion protection of the galvanic type. This is necessary to consider the thermal variation during the operation of the system. Magnesium anodes were chosen. Geometrical data and material specifications for the other components were taken from data sheets and materials readily available in the database, see Table 2.

Table 2. Hot water tank materials.

Material	Unit of Measure	Value	Notes
Stainless steel	kg	104.75	Value estimated from technical sheet
Aluminium	kg	4.4	Value estimated considering aluminium density, heat exchanger surface and thickness
Magnesium	kg	0.5	Literature data [34,35]
Rigid expanded polyurethane	kg	8.3	Estimated value considering data from the technical specifications of the water storage tank [36,37]
PVC	kg	1	Estimated plastic weight
Alkyd paint	kg	1.05	Estimated value considering water storage geomorphology, density, and paint thickness [38,39]

The life cycle assessment (LCA) also considers pipes, for conveying water from the receiver to the tank. The assumption here is that the hot water storage tank is positioned at 2 m from the receiver, and these pipes are constructed using polypropylene reinforced with fibreglass. External thermal insulation is applied to minimize heat losses, achieved using polyurethane. All the relevant data and technical specifications are sourced from a commercial data sheet, see Table 3.

Table 3. Piping system materials [40].

Material	Unit	Value	Notes
Polypropylene	kg	1.13	Estimated value from data sheet
Polyurethane	kg	1.45	Estimated value from data sheet

A cylindrical cavity receiver is used for its cost-effectiveness. The heat transfer surface of this receiver consists of a coiled copper metal tube. A heat transfer fluid flows within these coiled tubes to transfer the intense solar energy to the working fluid. The system presented here is designed to provide domestic hot water, with a temperature desired by the user of 45 °C. Thermia B oil, derived from highly refined mineral oils from crude oil, was chosen for this specific application. Considering the heat transfer tubes, a total of 20 litres of heat transfer fluid is required. To minimise heat loss from the cavity, the receiver of the cavity is assumed to be insulated with mineral wool insulation material, with a 20 mm thick layer of glass wool around the receiver, see Table 4.

Table 4. Solar receiver materials.

Material	Unit of Measure	Value	Notes
Copper	kg	11.2	Value estimated from receiver geometry considering a copper density of 8960 kg/m^3 [41]
AISI 310	kg	21.14	Value estimated from the geometry of the receiver, considering the density of AISI 310 to be 7900 kg/m^3 [42]
Glass wool	kg	0.122	Estimated value considering a wool density of 20 kg/m^3 [43]
Thermal oil	kg	17.36	Value estimated considering a thermal oil density equal to 868 kg/m^3 [44]

The geometrical parameters of the parabola used in the initial phase of this study mirror those of the parabola accessible at the Energy Center of the Politecnico di Torino. A thorough literature review was conducted, and some assumptions were made to complete the complete analysis of the system. Aluminium was chosen as the construction material for the solar dish (disc). The disc cover is 2 mm thick and is made of treated aluminium to increase reflection and concentration at the receiver. The support structure is made of stainless steel, see Table 5. There is a tracking mechanism and information about its construction support, and the materials used are available directly from the manufacturer [24]: the material used is Fe360 structural steel.

Table 5. Parabolic dish materials.

Material	Unit of Measure	Value	Notes
Stainless steel	kg	592.5	Value calculated considering the dish with a stainless steel density of 8000 kg/m^3 [45]
Aluminium	kg	320	Value estimated by calculating the area of the collector and its thickness, considering that the density of aluminium is 2710 kg/m^3 [46]
Glass	kg	20	Value estimated by calculating the collector area, with 2 mm glass thickness, assuming a glass density of 2500 kg/m^3 [47]
Structural steel	kg	0.9	Value calculated from the solar tracking system, considering the density of the structural steel to be 7850 kg/m^3 [48]

In the openLCA software (version 1.10.3), the disposal of products at the end of their life cycle is facilitated using flows categorized as "waste". These waste flows need to be incorporated into the process's output. The method employed for end-of-life treatment is known as the cut-off method. Under this approach, the model concludes with waste collection and treatment, excluding recycling and the creation of new products [49]. End-of-life treatment was implemented for several materials, including copper, glass wool, stainless steel, the hot water tank, and aluminium. However, for certain materials, modelling end-of-life scenarios proved challenging due to the limited data available in the database and the absence of suitable proxies for their treatment. The final process, "System Use," pertains to the production of a single hot water tank. This analysis assumes that the entire system can operate efficiently for 30 years. The system's utilization for water production is anticipated to occur daily, with the capacity to produce one tank of hot water (190 litres) available for 255 out of 365 days in a year, equivalent to 69.86% of the year's days. In terms of system lifetime, this translates to 10,950 days or 7650 operational days. Consequently, the production of one hot water tank contributes an equivalent of 0.000131.

The inputs of the utilisation phase include all the processes described above, including transport, as well as 190 litres of water. It is assumed that the entire system is produced at 500 km from the place of use and then transported by road with articulated lorries. Manual handling of the system was not considered due to the lack of available data on the subject. In summary, the use of the system includes the production of the solar collector, the production of the solar receiver, the production of the piping system, the production of the hot water storage tank, the transport from the place of production to the place of use, the actual use of the system, and the end-of-life disposal of the components.

3.2. Model and LCA Results

The choice of materials for the receiver was influenced by the maximum temperature derived from the Comsol multiphysics software.

This temperature is the result of the radiant flux striking the inner surfaces, sides, and bottom of the receiver after interception. When the radiant flux hits a particular surface, a fraction of it is absorbed and the rest is reflected onto the other surfaces, including the aperture. If it is reflected off the receiver wall, the process is repeated. If it is reflected to

the aperture, this fraction of radiant energy is lost to the environment—reflection losses. Reflection losses and reflection on the receiver surfaces depend on the following:

- Receiver shape and dimensions.
- The solar absorbance of the inner surfaces of the receiver. The type of reflection of the inner surfaces of the receiver, i.e., specular, specular with Gaussian scattering or Lambertian (diffuse).

Therefore, the heat flux absorbed by the receiver is non-uniformly distributed across its inner surfaces, and this distribution is influenced by various factors. In this analysis, the focal plane is defined as the inner cylinder with a radius of 150 mm and a height of 230 mm. The figure below illustrates the resulting temperature distribution (Figure 5).

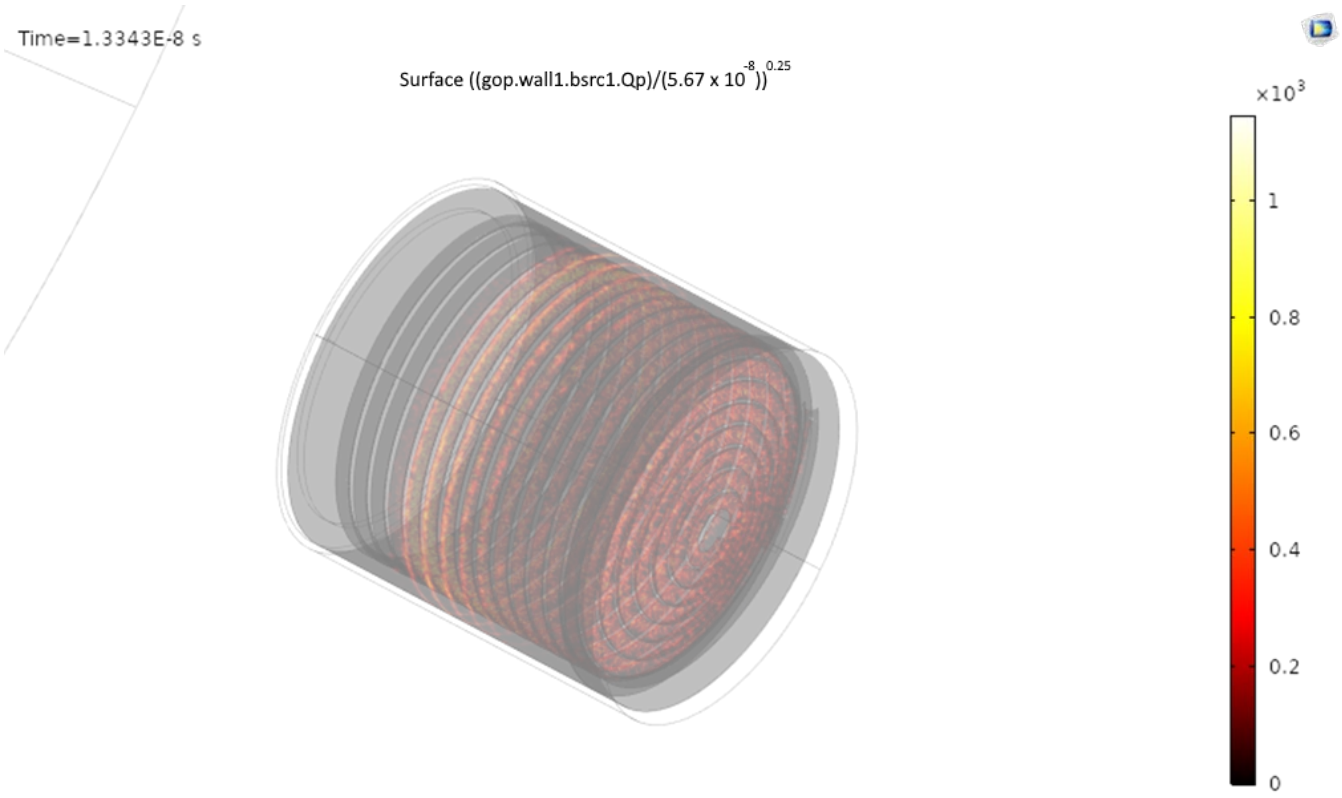

Figure 5. Temperature (K) distribution inside cavity receiver.

The highest attained temperature within the cavity receiver registers at 873.75 °C (or 1146.9 K), accompanied by an average power of 7466.7 $\frac{kW}{m^2}$. To endure this temperature, an internal coil made of copper tubes, consisting of fourteen turns along the cavity's height, is employed. Copper is chosen due to its rapid heat transfer capabilities, owing to its excellent thermal conductivity. Additionally, its affordability is a noteworthy advantage, especially for the household sector. The maximum temperature reached inside the cavity receiver is 873.7 °C (or 1146.9 K), accompanied by an average power of 7466.7 kW/m^2. As can be seen from the figure, the maximum temperature is only reached at certain points. The distribution reached is therefore compatible with the type of material (copper tubes with fourteen wound coils), and the maintenance of the receiver structure is guaranteed. Copper was chosen for its rapid heat transfer capabilities and excellent thermal conductivity, see Table 6.

Table 6. Copper properties.

Physical Parameter	Unit of Measure	Value
Density	kg/m^3	8960
Thermal conductivity	W/(mK)	386
Heat capacity at constant pressure	J/(kgK)	38

To improve the ability of the spirally wound copper tubes to effectively absorb solar radiation and reduce losses, it was decided to apply a black chrome coating to the copper surface $(Cr - Cr_2O_3)$. The black chrome coating has an emissivity of 0.09 and an absorbance of 0.84 [50]. The outer casing must be made of AISI 310 stainless steel, and the main properties of which are given in Table 7. AISI 310 is an austenitic stainless steel with a high chromium and nickel content and a high carbon content. This type of steel offers excellent heat resistance, although it has a significantly lower thermal conductivity than copper. As established above (Table 7), 7.71 kW is required to heat the water tank in one hour.

Table 7. AISI 310 properties.

Physical Parameter	Unit of Measure	Value
Density	kg/m^3	7900
Thermal conductivity	W/(mK)	23.7
Heat capacity at constant pressure	J/(kgK)	610

In the context of the presented system, approximately 5 h of radiation are required. This is based on an average heat source of 7.45 kW/m^2 inside the receiver, which has a surface area of 0.207 m^2. The system analysed for domestic hot water production operates without emissions during its use. However, emissions do occur during the production of these systems. The inventory collected for the life cycle assessment analysis includes all input and output components covering the entire life cycle of each modelled product. This inventory includes the flows of materials and energy exchanged between the system and the environment. Inputs are defined by the resources consumed, which include raw materials, energy, and land use, while outputs include emissions to air, water, or soil. Due to the large list of inputs and outputs, a cut-off value of 1% was applied. The result was 297 input components and 1890 output components. Below is a summary of the top 10 components for reference. Among the most used materials are hard coal, inert rock, water, natural gas, and crude oil, see Table 8.

These materials play a significant role in extraction and production processes. In contrast, other forms of renewable energy could be associated with the consumption of electricity during the production phase. The main pollutant emitted is carbon dioxide, which can be attributed to energy production, see Table 9.

Part of it comes from fossil fuels, while another part comes from the combustion or decomposition of organic materials.

The analysis of the impact of each component starts with the raw materials and includes the manufacturing phase, transport from the factory to the assembly site, and end-of-life treatment.

In the phase use, water consumption was added, while maintenance was not included due to lack of data. The climate change impact category is represented with the EF, i.e., Bern impact assessment model: Global Warming Potentials (GWPs) over a 100-year time horizon and the indicator are expressed in terms of kg of CO_2 equivalent. End-of-life treatment was applied to materials: copper, aluminium, steel, polyurethane, and glass wool (Figures 6–9) [51]. The results achieved are obtained from the openLCA 1.10.3 software.

Table 8. Inputs obtained from inventory analysis and referred to the functional unit of the system.

Input				
Flow	**Category**	**Sub-Category**	**Unit of Measure**	**Result**
Hard coal	Resources	From ground	MJ	3.9
Inert rock	Resources	From ground	kg	3.9
Water (rainwater)	Resources	From water	kg	2.8
Air	Resources	In air	kg	2.5
Natural gas	Resources	From ground	MJ	2.1
Crude oil	Resources	From ground	MJ	1.5
Sea water	Resources	From water	kg	1.5
Primary energy from hydro power	Resources	From water	MJ	0.75
Primary energy from solar energy	Resources	From air	MJ	0.3
Uranium	Resources	From ground	MJ	0.27

Table 9. Emissions to air and water of the main pollutants were obtained from inventory analysis and referred to the functional unit of the system (openLCA 1.10.3).

Emissions				
Flow	**Category**	**Sub-category**	**Unit of Measure**	**Result**
Carbon dioxide (fossil)	Emissions	Emissions to air	kg	0.65
Carbon dioxide (biogenic)	Emissions	Emissions to air	kg	0.0226
Sulphur dioxide	Emissions	Emissions to air	kg	0.0031
Nitrogen dioxide	Emissions	Emissions to air	kg	0.00145
Carbon monoxide (fossil)	Emissions	Emissions to air	kg	0.00126
Nitrogen monoxide	Emissions	Emissions to air	kg	0.000056
Nitrous oxide	Emissions	Emissions to air	kg	0.000011
Nitrogen oxides	Emissions	Emissions to air	kg	0.0000092
Carbon monoxide (biogenic)	Emissions	Emissions to air	kg	0.0000014
Sulphate	Emissions	Emissions to air	kg	0.00000039

In all processes, except pipeline pipes, stainless steel production stands out as the most significant contributor to the climate change impact category. For both steel production technologies, hot-rolling and cold-rolling, the available data set includes all relevant stages of supply, with the process inventory based mainly on industrial data. The data set for steel production is based on internationally recognised production processes and linked to regional precursors. Although steel production is known for its energy intensity and significant greenhouse gas emissions, it is important to note that steel can be recycled. However, it should be noted that this analysis does not consider recycled steel as input material.

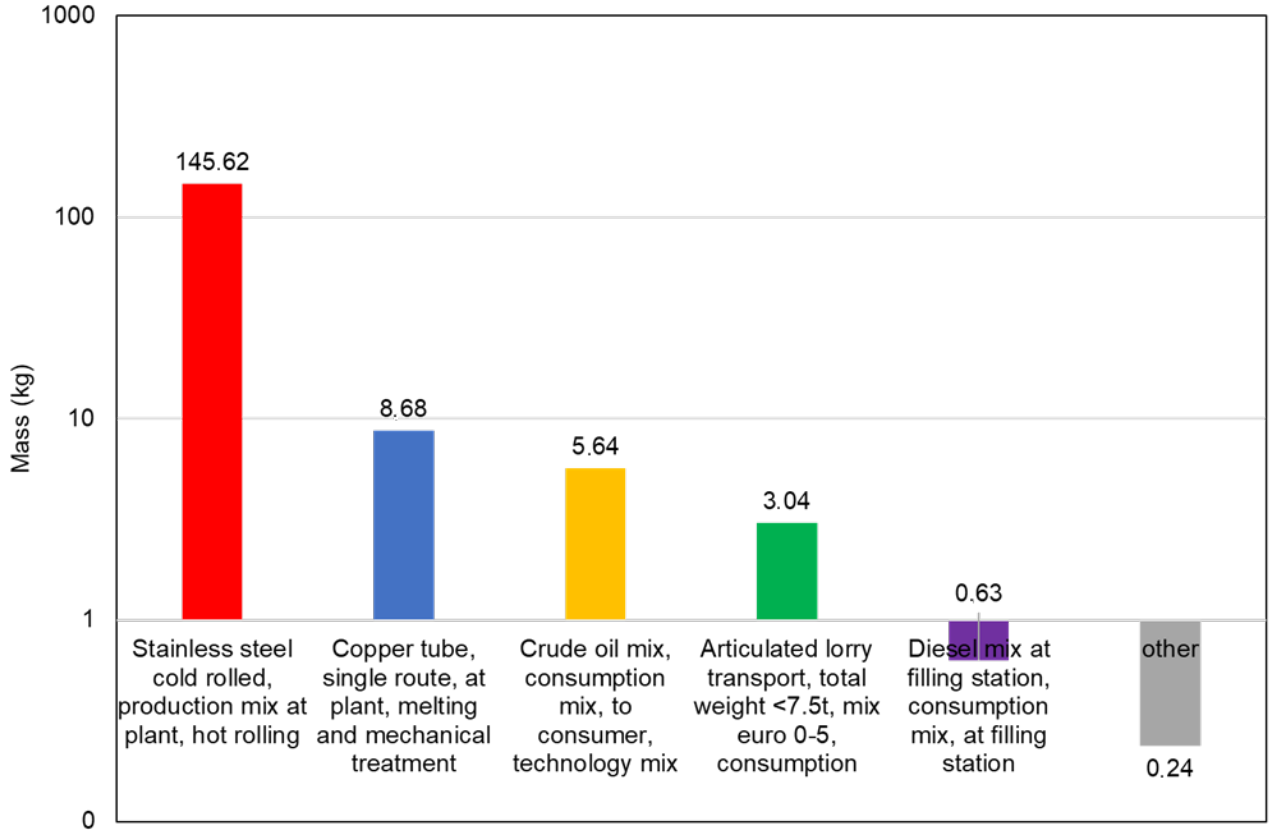

Figure 6. Climate change impact category for the production of cavity solar receivers.

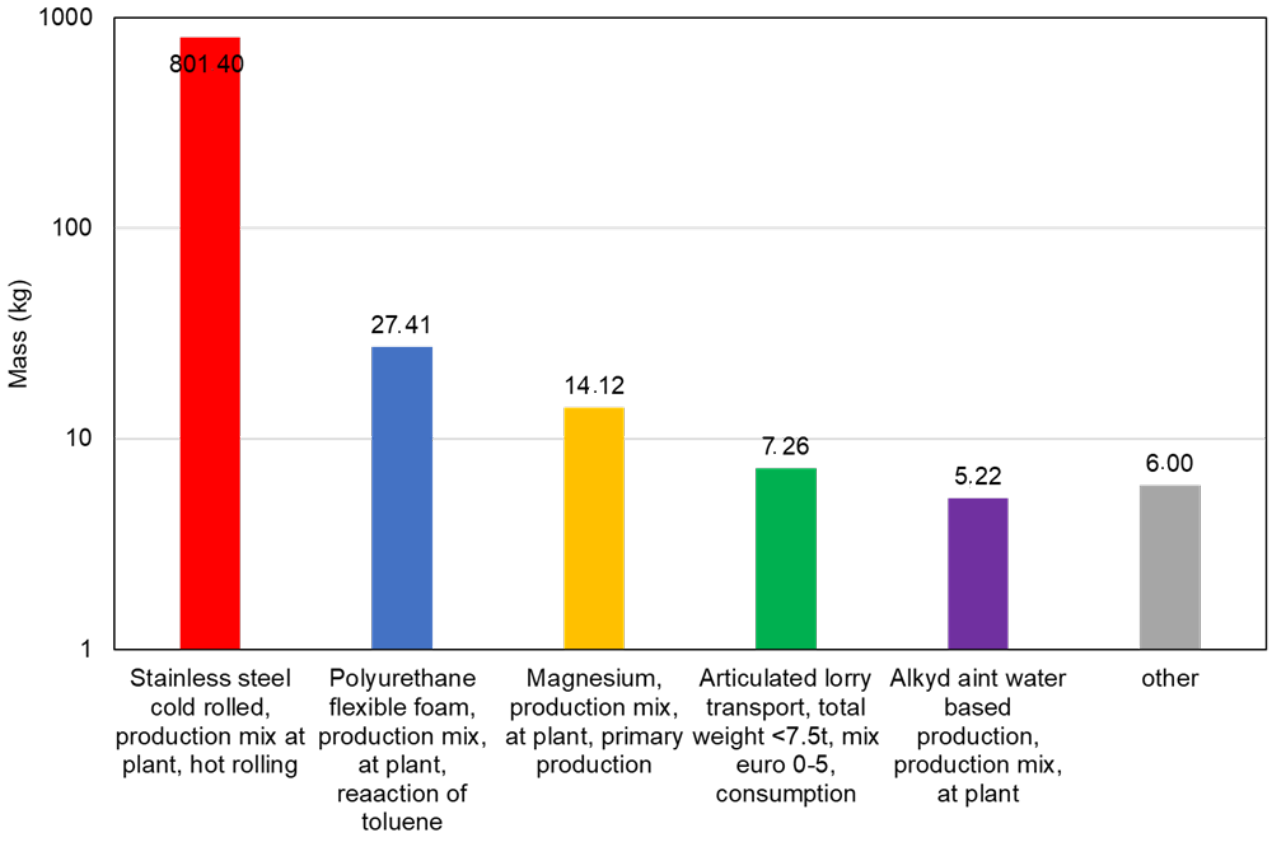

Figure 7. Climate change impact category for hot water tank production.

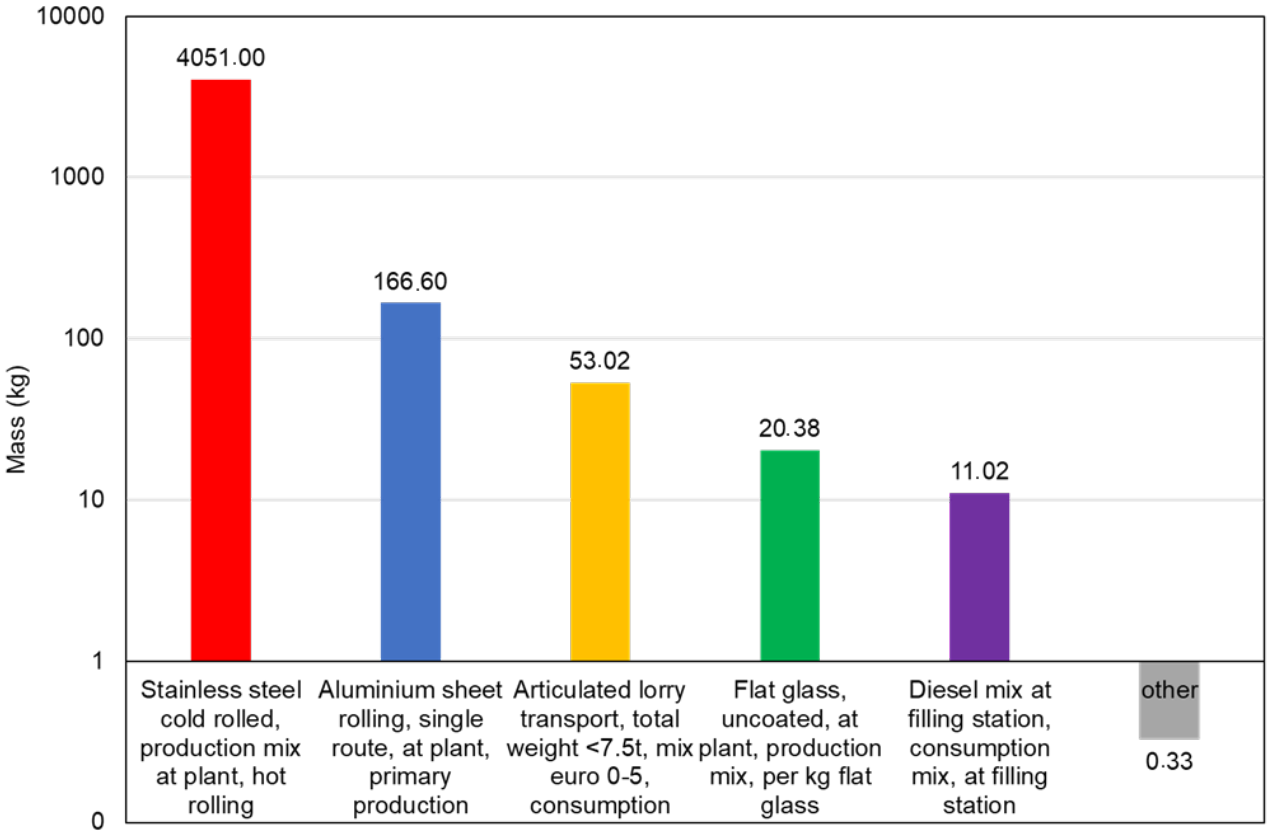

Figure 8. Climate change impact category for solar dish production.

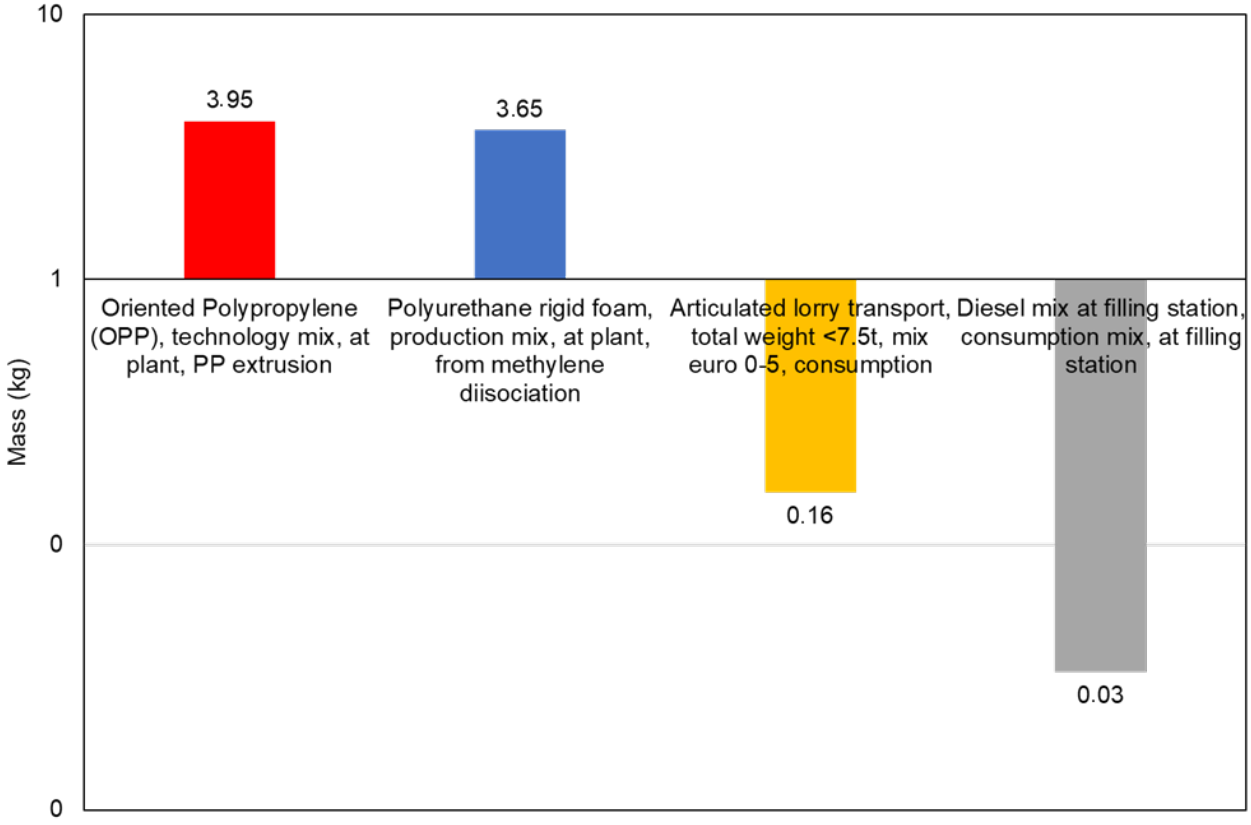

Figure 9. Climate change impact category for pipeline production.

The process with the most significant impact in all categories, except for ozone depletion, is the manufacture of the dish, see Table 10. Steel stands out as the least environmentally friendly material due to its energy-intensive production. This observation extends to other impact categories, and since satellite dishes contain a substantial amount of steel, they also emerge as the main contributors to these impact categories. In contrast, for the ozone depletion indicator, the pipe manufacturing process takes the lead. This contribution can be attributed to the use of polyurethane as an insulating material. The available data set for this material covers the entire life cycle and the inventory comes from European industry data (EU-28 + EFTA, (openLCA 1.10.3)). The same amount of domestic hot water could be heated with a conventional natural gas boiler. Assuming a boiler efficiency of 93% and stoichiometric methane consumption, 1.6 kg of CO_2 will be emitted in one day. Assuming the same emissions for 30 years and considering the same number of days of operation of the solar dish, 12,240 kg of CO_2 is emitted. This number results only from the operation phase of the system and is much larger than the number obtained from the production process of the four components of the solar dish analysed above. Assuming the same emissions over the life cycle and considering the days when the solar antenna is in operation, 12,240 kg CO_2 is emitted. This number comes only from the operation phase of the system and is much larger than that obtained from the production process of the four solar antenna components analysed above.

Table 10. Comparison of the analysed components for the different impact categories, source openLCA 1.10.3.

Indicator	Parabolic Dish	Hot Water Tank	Cavity Receiver	Piping Line	Unit of Measure
Acidification	32.303	6.413	1.242	0.017	mol H^+ eq
Climate change	4300	861	164	7.79	kg CO_2 eq
Ecotoxicity, freshwater	2610	545	105	1.16	CTUe
Eutrophication, freshwater	0.0051	0.00156	0.00018	0.0000362	kg P eq
Human toxicity, cancer	0.000049	0.0000103	0.00000208	0.000000068	CTUh
Human toxicity, non-cancer	0.00019	0.0000643	0.000000135	0.00000068	CTUh
Ionising radiation, human health	75.4	10.3	3.02	414	kg U235 eq
Land use	5820	1180	197	29.6	
Ozone depletion	0.000000068	0.000000317	0.0000000025	0.00000667	kg CFC-11 eq
Particulate matter	0.000518	0.000104	0.0000185	0.00000015	kg PM2.5 eq
Photochemical ozone formation	11.9	2.33	0.466	0.014	kg NMVOC eq
Resource use, fossil	49,100	10,000	2580	193	MJ
Resource use, minerals, and metals	0.0208	0.0410	0.00000808	0.0000035	kg Sb eq
Water use	1270	259	42.1	1.42	m^3

4. Conclusions

This study evaluates a thermal energy production system using a concentrated solar power plant. The system runs on renewable solar energy, making its operational phase sustainable. However, the production phase involves non-renewable resources and emissions. In the first part, the geometry of the cavity receiver was analysed using the Comsol

multiphysics software to select the materials. A cylindrical cavity receiver was chosen, considering a balance between cost and efficiency. Copper was chosen for the heat transfer tubes due to its high thermal conductivity and cost-effectiveness. The outer casing of the cavity receiver is made of AISI 310 steel to withstand high temperature but has a lower thermal conductivity than copper. It is insulated with 20 mm glass wool to minimise heat loss. The second part of the study considered the life cycle assessment (LCA) of the hot water production system using the openLCA software. The LCA utilised four main components: the solar dish, the solar receiver, the piping system, and the hot water tank. The materials for each component were selected based on commercial offers and scientific publications. For each component, the entire life cycle, including transport, was modelled.

The LCA analysis explored various impact categories, highlighting stainless steel as the most polluting material among the selected components. Emissions could be reduced by using recycled materials. Despite emissions during the production phase, the solar cooker represents a promising alternative to conventional hot water production systems. The study reveals that CO^2 emissions during the operational phase of conventional systems exceed those from the production of the four analysed components combined. Technological advances have the potential to improve the cost-effectiveness and environmental compatibility of these systems. However, to fully quantify the environmental impact of renewable energy systems, further research in the field of life cycle assessment (LCA) is needed.

Author Contributions: I.T., writing the original draft, data curation, conduct of research, modelling activity; D.P. supervision, revising the final version, research idea. All authors have read and agreed to the published version of the manuscript.

Funding: This research received no external funding.

Data Availability Statement: Data will be provided upon request.

Conflicts of Interest: The authors declare no conflict of interest.

Nomenclature

A	Area of the concentrator (m^2)
cp	Water's specific heat (kJ/kg/K)
Co	Optical concentration ratio (-)
CSP	Concentrated solar power
CSR	Circumsolar ratio
D_c	Diameter of the dish (mm)
d_f	Diameter of the focal point (mm)
DHW	Domestic hot water
E	Thermal energy for the sensible storage
f	Focal distance (mm)
GHG	Greenhouse gases
l	Length of the receiver (mm)
LCA	Life cycle assessment
P	Power of the concentrator (kW)
q	Heat flux (W/m^2)
Q	Incoming solar power (kW)
SC	Solar concentrator
SDH	Solar district heating
TES	Thermal energy storage
Tmains	Aqueduct temperature (°C)
Tmax	Maximum temperature in the tank (°C)
Tmin	Minimum temperature (°C)
Tuse	Desired temperature in the tank (°C)
V	Tank volume for the sensible storage

φ_R	Rim angle (°)
y_R	Depth (mm)
ρ	Density (kg/m^3)

References

1. Delivering the European Green Deal. 2021. Available online: https://commission.europa.eu/strategy-and-policy/priorities-2019-2024/european-green-deal/delivering-european-green-deal_en (accessed on 14 November 2023).
2. McKinsey. Five Key Areas for Europe's Energy Transition. (n.d.). Available online: https://www.mckinsey.com/capabilities/sustainability/our-insights/five-key-action-areas-to-put-europes-energy-transition-on-a-more-orderly-path (accessed on 14 November 2023).
3. Gielen, D.; Boshell, F.; Saygin, D.; Bazilian, M.D.; Wagner, N.; Gorini, R. The role of renewable energy in the global energy transformation. *Energy Strategy Rev.* **2019**, *24*, 38–50. [CrossRef]
4. Hafner, M.; Tagliapietra, S. The Global Energy Transition: A Review of the Existing Literature. In *The Geopolitics of the Global Energy Transition*; Hafner, M., Tagliapietra, S., Eds.; Springer International Publishing: Cham, Switzerland, 2020; pp. 1–24. [CrossRef]
5. IREES—Institut Für Ressourceneffizienz und Energiestrategien GmbH. Comprehensive Assessment of the Potential for Efficient Heating and Cooling for Germany, (n.d.). Available online: https://energy.ec.europa.eu/system/files/2022-05/DE%20CA%202020%20en.pdf (accessed on 14 November 2023).
6. IEA. Heating, (n.d.). Available online: https://www.iea.org/energy-system/buildings/heating (accessed on 3 November 2023).
7. Mapping and Analyses of the Current and Future (2020–2030) Heating/Cooling Fuel Deployment (Fossil/Renewables), (n.d.). Available online: https://energy.ec.europa.eu/publications/mapping-and-analyses-current-and-future-2020-2030-heatingcooling-fuel-deployment-fossilrenewables-1_en (accessed on 3 November 2023).
8. Temiz, M.; Dincer, I. Development and assessment of an onshore wind and concentrated solar based power, heat, cooling and hydrogen energy system for remote communities. *J. Clean. Prod.* **2022**, *374*, 134067. [CrossRef]
9. Krajačić, G.; Vujanović, M.; Duić, N.; Kılkış, Ş.; Rosen, M.A.; Al-Nimr, M.A. Integrated approach for sustainable development of energy, water and environment systems. *Energy Convers. Manag.* **2018**, *159*, 398–412. [CrossRef]
10. N'tsoukpoe, K.E.; Lekombo, S.C.; Kemausuor, F.; Ko, G.K.; Diaw, E.H.B. Overview of solar thermal technology development and applications in West Africa: Focus on hot water and its applications. *Sci. Afr.* **2023**, *21*, e01752. [CrossRef]
11. Hafez, A.; Soliman, A.; El-Metwally, K.; Ismail, I. Design analysis factors and specifications of solar dish technologies for different systems and applications. *Renew. Sustain. Energy Rev.* **2017**, *67*, 1019–1036. [CrossRef]
12. Task 55. IEA SHC, Integration of Large SHC Systems into DHC Networks, (n.d.). Available online: https://task55.iea-shc.org/ (accessed on 3 November 2023).
13. Abid, M.; Khan, M.S.; Ratlamwala, T.A.H. Thermodynamic Performance Evaluation of a Solar Parabolic Dish Assisted Multigeneration System. *J. Sol. Energy Eng.* **2019**, *141*, 061014. [CrossRef]
14. Reddy, K.; Veershetty, G.; Vikram, T.S. Effect of wind speed and direction on convective heat losses from solar parabolic dish modified cavity receiver. *Sol. Energy* **2016**, *131*, 183–198. [CrossRef]
15. Coventry, J.; Andraka, C. Dish systems for CSP. *Sol. Energy* **2017**, *152*, 140–170. [CrossRef]
16. Bianchini, A.; Guzzini, A.; Pellegrini, M.; Saccani, C. Performance assessment of a solar parabolic dish for domestic use based on experimental measurements. *Renew. Energy* **2019**, *133*, 382–392. [CrossRef]
17. Wang, M.; Siddiqui, K. The impact of geometrical parameters on the thermal performance of a solar receiver of dish-type concentrated solar energy system. *Renew. Energy* **2010**, *35*, 2501–2513. [CrossRef]
18. Abbas, S.; Yuan, Y.; Hassan, A.; Zhou, J.; Ahmed, A.; Yang, L.; Bisengimana, E. Effect of the concentration ratio on the thermal performance of a conical cavity tube receiver for a solar parabolic dish concentrator system. *Appl. Therm. Eng.* **2023**, *227*, 120403. [CrossRef]
19. Marra, A.; Santarelli, M.; Papurello, D. Solar Dish Concentrator: A Case Study at the Energy Center Rooftop. *Int. J. Energy Res.* **2023**, *2023*, 9658091. [CrossRef]
20. Papurello, D.; Bertino, D.; Santarelli, M. CFD Performance Analysis of a Dish-Stirling System for Microgeneration. *Processes* **2021**, *9*, 1142. [CrossRef]
21. Borghero, L.; Bressan, M.; Ferrero, D.; Santarelli, M.; Papurello, D. Methane-Assisted Iron Oxides Chemical Looping in a Solar Concentrator: A Real Case Study. *Catalysts* **2022**, *12*, 1477. [CrossRef]
22. Montà, E.; Santarelli, M.; Papurello, D. Synthetic-Gas Production through Chemical Looping Process with Concentrating Solar Dish: Temperature-Distribution Evaluation. *Processes* **2022**, *10*, 1698. [CrossRef]
23. Perrero, M.; Papurello, D. Solar Disc Concentrator: Material Selection for the Receiver. *Energies* **2023**, *16*, 6870. [CrossRef]
24. El. *Ma Electronic Machining S.R.L. Manuale Uso e Manutenzione—Concentratore Solare a Disco*; El.Ma Electronic Machining S.R.L.: Riva del Garda, Italy, 2019.
25. COMSOL. How to Model Solar Concentrators with the Ray Optics Module, (n.d.). Available online: https://www.comsol.it/blogs/how-to-model-solar-concentrators-with-the-ray-optics-module/ (accessed on 20 June 2022).
26. 2_termocoppie_kXMVjwz.pdf, (n.d.). Available online: https://www.tersid.it/files/documentoprodotto/2020/2_termocoppie_kXMVjwz.pdf (accessed on 18 December 2023).

27. Tursunovic, I.; Papurello, D. Design of a Receiver for Solar Parabolic Dish and Life Cycle Assessment of Domestic Hot Water Production System. Master's Thesis, Politecnico di Torino, Torino, Italy, 2022.
28. Cabeza, L.F.; Martorell, I.; Miró, L.; Fernández, A.; Barreneche, C. Introduction to thermal energy storage (TES) systems. In *Advances in Thermal Energy Storage Systems*; Woodhead Publishing: Sawston, UK, 2015; pp. 1–28. [CrossRef]
29. Corona, B.; Miguel, G.S. Life cycle sustainability analysis applied to an innovative configuration of concentrated solar power. *Int. J. Life Cycle Assess.* **2019**, *24*, 1444–1460. [CrossRef]
30. Piemonte, V.; De Falco, M.; Tarquini, P.; Giaconia, A. Life Cycle Assessment of a high temperature molten salt concentrated solar power plant. *Sol. Energy* **2011**, *85*, 1101–1108. [CrossRef]
31. Ko, N.; Lorenz, M.; Horn, R.; Krieg, H.; Baumann, M. Sustainability Assessment of Concentrated Solar Power (CSP) Tower Plants—Integrating LCA, LCC and LCWE in One Framework. *Procedia CIRP* **2018**, *69*, 395–400. [CrossRef]
32. Lamnatou, C.; Chemisana, D. Concentrating solar systems: Life Cycle Assessment (LCA) and environmental issues. *Renew. Sustain. Energy Rev.* **2017**, *78*, 916–932. [CrossRef]
33. Carnevale, E.; Lombardi, L.; Zanchi, L. Life Cycle Assessment of solar energy systems: Comparison of photovoltaic and water thermal heater at domestic scale. *Energy* **2014**, *77*, 434–446. [CrossRef]
34. ScienceDirect Topics. Cathodic Protection—An Overview, (n.d.). Available online: https://www.sciencedirect.com/topics/physics-and-astronomy/cathodic-protection (accessed on 15 November 2023).
35. Pathak, S.S.; Mendon, S.K.; Blanton, M.D.; Rawlins, J.W. Magnesium-Based Sacrificial Anode Cathodic Protection Coatings (Mg-Rich Primers) for Aluminum Alloys. *Metals* **2012**, *2*, 353–376. [CrossRef]
36. EMMETI-Catalogo-Tecnico-Bollitori-e-Serbatoi-ad-Accumulo-2019.pdf, (n.d.). Available online: https://www.schede-tecniche.it/schede-tecniche-bollitori/EMMETI-catalogo-tecnico-bollitori-e-serbatoi-ad-accumulo-2019.pdf (accessed on 15 November 2023).
37. Fiorini Industries. Rigid Expanded Polyurethane Water Storage Tank Data Sheet—Fiorini Industries, (n.d.). Available online: https://www.fiorini-industries.com/en/download/root/eng/product_data_sheets_2018_rev1/without_prices/hot_water_storage_tanks.pdf (accessed on 15 November 2023).
38. Interline-850-Potable-Water-Tanks.pdf, (n.d.). Available online: https://marinecoatings.brand.akzonobel.com/m/2daa08217affb122/original/Interline-850-Potable-Water-Tanks.pdf (accessed on 15 November 2023).
39. Scribd. Alkydprimer: Technical Data Sheet | PDF | Abrasive | Paint, (n.d.). Available online: https://www.scribd.com/document/518722084/Download-2 (accessed on 15 November 2023).
40. IDROTHERM-2000-Catalogo-Listino.pdf, (n.d.). Available online: https://agenzia-estesa.it/wp-content/uploads/2021/01/IDROTHERM-2000-Catalogo-Listino.pdf (accessed on 15 November 2023).
41. Copper—Element information, properties and uses | Periodic Table, (n.d.). Available online: https://www.rsc.org/periodic-table/element/29/copper (accessed on 15 November 2023).
42. Materials UK. Stainless Steel 310—1.4845 Data Sheet, (n.d.). Available online: https://www.thyssenkrupp-materials.co.uk/stainless-steel-310-14845.html (accessed on 15 November 2023).
43. ISOVER, SUIS_GB_Glass-wool_2016-03. 2016. Available online: https://www.isover-technical-insulation.com/documents/suis-sds/suis-glasswool.pdf (accessed on 15 November 2023).
44. Shell Thermia, THERMIA-B.pdf, (n.d.). Available online: https://www.yairerez.co.il/wp-content/uploads/2019/10/THERMIA-B.pdf (accessed on 15 November 2023).
45. Density of Steel—The Physics Factbook, (n.d.). Available online: https://hypertextbook.com/facts/2004/KarenSutherland.shtml (accessed on 15 November 2023).
46. Materials UK. The Density of Aluminium and Its Alloys—Thyssenkrupp Materials (UK), (n.d.). Available online: https://www.thyssenkrupp-materials.co.uk/density-of-aluminium.html (accessed on 15 November 2023).
47. Saint Gobain Building Glass UK. Physical Properties of Glass, (n.d.). Available online: https://www.saint-gobain-glass.co.uk/en-gb/architects/physical-properties (accessed on 15 November 2023).
48. Fe Grade Steels, (n.d.). Available online: https://www.geocentrix.co.uk/help/content/items/steels/fe_grade_steels.htm (accessed on 15 November 2023).
49. Nordelöf, A.; Poulikidou, S.; Chordia, M.; de Oliveira, F.B.; Tivander, J.; Arvidsson, R. Methodological Approaches to End-Of-Life Modelling in Life Cycle Assessments of Lithium-Ion Batteries. *Batteries* **2019**, *5*, 51. [CrossRef]
50. Hassan, A.; Quanfang, C.; Abbas, S.; Lu, W.; Youming, L. An experimental investigation on thermal and optical analysis of cylindrical and conical cavity copper tube receivers design for solar dish concentrator. *Renew. Energy* **2021**, *179*, 1849–1864. [CrossRef]
51. Andreasi, B.S.; Biganzoli, F.; Ferrara, N.; Amadei, A.; Valente, A.; Sala, S.; Ardente, F. Updated characterisation and normalisation factors for the Environmental Footprint 3.1 method. In *JRC Publications Repository*; Publications Office of the European Union: Luxembourg, 2023. [CrossRef]